

This paper was accepted to the
Workshop on the Algorithmic Foundations of Robotics (WAFR), 2024.

Exploiting Chordal Sparsity for Fast Global Optimality with Application to Localization

Frederike Dümbsgen¹[0000–0002–7258–9753], Connor Holmes²[0000–0002–8314–3677],
and Timothy D. Barfoot²[0000–0003–3899–631X]

¹ Inria, Ecole Normale Supérieure, PSL University, Paris, France
<https://willow.inria.fr>
frederike.dumbgen@inria.fr

² University of Toronto, Robotics Institute, Toronto ON M3H5T6, Canada
<https://robotics.utoronto.ca>

Abstract. In recent years, many estimation problems in robotics have been shown to be solvable to global optimality using their semidefinite relaxations. However, the runtime complexity of off-the-shelf semidefinite programming (SDP) solvers is up to cubic in problem size, which inhibits real-time solutions of problems involving large state dimensions. We show that for a large class of problems, namely those with chordal sparsity, we can reduce the complexity of these solvers to linear in problem size. In particular, we show how to replace the large positive-semidefinite variable with a number of smaller interconnected ones using the well-known chordal decomposition. This formulation also allows for the straightforward application of the alternating direction method of multipliers (ADMM), which can exploit parallelism for increased scalability. We show for two example problems in simulation that the chordal solvers provide a significant speed-up over standard SDP solvers, and that global optimality is crucial in the absence of good initializations.

Keywords: Control Theory and Optimization · Localization and Mapping · Multi-Agent Systems and Distributed Robotics.

1 Introduction

To this date, optimization problems in robotics are predominantly solved with fast local methods. Popular choices in state estimation, for example, are Gauss-Newton (GN) [5], or incremental smoothing and mapping (iSAM) [29, 30]; planning and control problems are commonly solved with sequential quadratic programming algorithms and variants thereof [45]. Because the cost can become non-convex as soon as non-linear measurement models, dynamic models, or other non-convex constraints are employed, these methods may converge to poor local minima in the absence of well-informed initializations.

In recent years, important advances have been made towards globally optimal solvers. In computer vision, rotation averaging and registration problems [31, 23, 21] have been globally solved first, followed more recently by methods for optimal outlier-robust estimation [56]. Classical robotics problems such

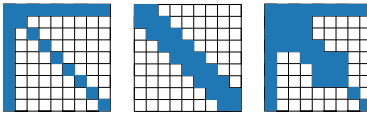


Fig. 1. By the nature of variable dependencies in many robotics problems, core matrices (e.g., inverse covariance matrices in state estimation) will have particular sparsity patterns. Examples are arrowhead (left), band-sparse (middle), and mixed (right) matrices, for which state-of-the-art (local) solvers achieve linear complexity. In this paper, we explain how SDP solvers can also yield linear complexity by exploiting chordal (aggregate) sparsity [58].

as range-only localization [20, 26] and range-aided simultaneous localization and mapping (SLAM) [42], pose-graph optimization [47, 11], and isotropic [27] or non-isotropic [28] SLAM have also seen adaptations of global solvers. We are even seeing a surge of globally optimal solvers for planning problems [35, 15].

In many of the aforementioned global methods, the computational bottleneck lies in solving a high-dimensional SDP. Off-the-shelf solvers for solving SDPs commonly use interior-point methods [37], which are of approximately cubic complexity in the number of unknowns and constraints [1]. This compares favorably with worst-case exponential-time methods such as branch and bound [39]. However, in order to be competitive with efficient local solvers [5, 30], more efficient SDP solvers are desired. Indeed, by exploiting sparsity, state-of-the-art local solvers can run in linear time in either the number of unknown landmarks or poses and, thanks to sophisticated handling of computation graphs, can update solutions efficiently in an online manner [30].

In this paper, we use well-established tools from the optimization community [8, 54] to show how SDP solvers can also be significantly sped up by exploiting sparsity. For a particular class of problems, namely problems with chordal sparsity (see Figure 1), the SDP can be decomposed into interconnected smaller problems. This not only reduces the computational complexity of solving the SDP but also allows for the problem to be distributed across many computational cores using, for example, the alternating direction method of multipliers (ADMM). We show that such decompositions allow the solver complexity to be reduced to approximately *linear* in the number of variables, which is a significant speedup and comparable to efficient but initialization-dependent *local* solvers. In summary, our contributions are as follows.

- We adopt the decomposed SDP (dSDP) solver [58] for the semidefinite relaxations of robotic localization problems, designing an intuitive factor-graph language for modeling.
- We investigate the distributed implementation of dSDP, using standard consensus ADMM. We call the resulting decentralized algorithm dSDP-admm.
- We showcase the performance of the methods on two classical localization problems, which both satisfy the chordal sparsity assumptions and empirically show that they have the same complexity as efficient *local* solvers. In particular, we emphasize the importance of redundant constraints, which may be required to improve the tightness of the semidefinite relaxation but

may also reduce the aggregate sparsity. This, in turn, impacts how well the problem may be decomposed.

We emphasize that the proposed methods have been considered in the control community [59], and applied for example for optimal power flow [17]. Our contribution lies in adopting them for state estimation problems and by using the factor-graph language [18], opening the door to their broader application in robotics. We also pay particular attention to redundant constraints, which are commonly required for tightness and may significantly impact the solver’s effectiveness.

This paper is structured as follows. We give an overview of related work and important graph-theoretic identities in Sections 2 and 3, respectively. In Section 4, we present the methodology to pass from the original sparse non-convex problem to the convex relaxation, design the factor-graph framework to describe and decompose such problems, and finally discuss the sparsity-exploiting solvers. We demonstrate the performance of the two proposed methods on two localization problems in Section 5 and conclude in Section 6.

2 Related Work

The proposed methods lie at the intersection of two active research areas in robotics: distributed algorithms and efficient globally optimal solvers.

Distributed algorithms allow for increased efficiency thanks to parallelism and load sharing. Examples are multi-core implementations for control, where open source packages such as OSQP [49] and ProxQP [3, 4] use ADMM and proximal methods of multipliers, respectively, for solving quadratic programs efficiently. In estimation, [22] uses a majorization minimization technique to enable the multi-core solution of large-scale bundle adjustment, while [41] proposes the use of Gaussian belief propagation on dedicated hardware to speed up the same problem. Distributed algorithms also have the advantage that they can be shared across multiple robots, allowing for collaborative solutions, such as mapping with multiple robots [12, 13], where particular attention has been given to limited communication bandwidth and proximity constraints [16, 14, 36].

All aforementioned solvers still distribute a *local* solver and may thus converge to poor local minima. For a number of problems, including landmark-based SLAM and pose-graph optimization, it has been shown that global solvers can be derived [11, 47, 27], and the distributed extension of such solvers is thus of interest. First steps in this direction have been taken in [53, 52], where the Burer-Monteiro-based method from [47] is applied in a distributed setting. The practicality of the approach has been demonstrated by its adoption in a distributed semantic SLAM framework [51]. To this date, the Burer-Monteiro methods have not been successfully applied to problems that require so-called redundant constraints. However, in many instances in robotics [57, 56, 55, 28, 19, 7, 26], redundant constraints are paramount to achieve tight semidefinite relaxations and thus globally optimal solutions.

We take a different route and investigate exploiting sparsity in general-purpose SDP solvers, which may be more suited to deal with redundant constraints. Summaries of existing methods are provided in the monograph by [54] and the recent survey paper by [58]. First, sparsity can be exploited in the inner iterations of interior-point solvers, using, for example, sparse matrix decompositions. One other notable example is the *Splitting Conic Solver* [38], which can exploit sparsity through a matrix-free and even a GPU-supported version. In [21], and for the specific problem of rotation averaging, the authors use block-coordinate descent on the positive semidefinite variable, updating one row at a time. The algorithm is improved in [43] by updating instead one rotation matrix at a time, which allows for the seamless integration of a local solver, which empirically greatly improves convergence. Different in nature are so-called decomposition methods for SDPs, which are the subject of this paper; here, the sparsity is exploited to reduce the problem to many smaller-sized instances that can either be solved in one shot [24, 33] or in an alternating way [32, 50]. We show in this paper that many state estimation problems are in fact suitable candidates for these methods, provided that redundant constraints are such that chordal sparsity is not affected significantly.

3 Background

3.1 Notation and definitions

We denote scalars, vectors, matrices, and sets, respectively, by the fonts x , \mathbf{x} , \mathbf{X} , and \mathcal{X} . The j -th element of a vector, the j -th column of a matrix, and the element (i, j) of a matrix are denoted, respectively, by $\mathbf{x}[j]$, $\mathbf{X}[j]$, and $\mathbf{X}[i, j]$. We write $\mathbf{X} \succeq 0$ to mean \mathbf{X} is positive semidefinite. \mathbf{I}_d is the identity matrix of size d , and d is dropped when clear from context. Similarly, $\mathbf{0}_d$ and $\mathbf{1}_d$ are vectors of all zeros or all ones, respectively. The operator $\text{vech}(\cdot)$ returns the vectorized version of the upper-diagonal part of a symmetric matrix \mathbf{X} , where off-diagonal elements are multiplied by $\sqrt{2}$, ensuring $\text{tr}(\mathbf{Q}^\top \mathbf{X}) = \text{vech}(\mathbf{Q})^\top \text{vech}(\mathbf{X})$. We denote the inverse operation by $\text{mat}(\cdot)$: $\mathbf{X} = \text{mat}(\mathbf{y})$ and we write $\mathbf{y} \succeq 0$ to mean $\text{mat}(\mathbf{y}) \succeq 0$.

An undirected graph is defined as $\mathcal{G} = (\mathcal{V}, \mathcal{E})$, where \mathcal{V} is the set of vertices and \mathcal{E} is the set of edges. We use $(i, j) \in \mathcal{E}$ and $(i, j) \in \mathcal{G}$ interchangeably, as well as $i \in \mathcal{V}$ and $i \in \mathcal{G}$. A *subgraph* induced by a set of vertices $\mathcal{W} \subset \mathcal{V}$ is the graph with vertices \mathcal{W} and edges $\mathcal{E} \cap (\mathcal{W} \times \mathcal{W})$. A *clique* is a subgraph that is fully connected. A *cycle* is a set of pairwise distinct vertices $v_1, v_2, \dots, v_k \subset \mathcal{V}$ such that $(v_1, v_k) \in \mathcal{E}$ and $(v_i, v_{i+1}) \in \mathcal{E}$. A *chord* in a cycle is an edge connecting two non-consecutive vertices.

3.2 Chordal sparsity in SDPs

An extensive treatment of sparsity in semidefinite programming is given in [58]. Here, we introduce some lighter notation and highlight the concepts that will be the most useful to us in the remainder of the paper.

Given a set of symmetric matrices $\mathcal{A} = \{\mathbf{A}_1, \dots, \mathbf{A}_K\}$, we define the *aggregate sparsity pattern* of \mathcal{A} as the following set of pairwise indices:

$$\mathcal{E} = \{(i, j) \mid \exists \mathbf{A}_k \in \mathcal{A} \text{ s.t. } \mathbf{A}_k[i, j] \neq 0\}. \quad (1)$$

In other words, this is the set of all index pairs at which at least one of the matrices in the set has a non-zero element. We define the *sparsity graph* of \mathcal{A} as $\mathcal{G} = (\{1, \dots, N\}, \mathcal{E})$. Next, we reiterate a few well-known properties of graphs.

Definition 1 (Chordal graph). *A graph \mathcal{G} is chordal if every cycle of length ≥ 4 contains at least one chord.*

A graph can be rendered chordal by simply adding edges until it is chordal. Finding the minimum chordal extension, i.e., the minimum set of chords to render the graph chordal, is an NP-hard problem, but efficient heuristics exist [58]. In this paper, we will make use of specific sparsity patterns that typically arise in robotics applications and use deterministic chordal extensions.

Definition 2 (Maximal clique). *\mathcal{C} is a maximal clique of \mathcal{G} if it is not contained in any other clique of \mathcal{G} .*

Finally, we say that a matrix is semidefinite-completable in \mathcal{E} , written as $\mathbf{X}_{\mathcal{E}} \succeq 0$, if \mathbf{X} can be made positive semidefinite by changing only the elements corresponding to indices *not* in \mathcal{E} .

Now, we can state the important property that enables us to replace the large SDP variable with smaller ones. We consider SDPs of the general form

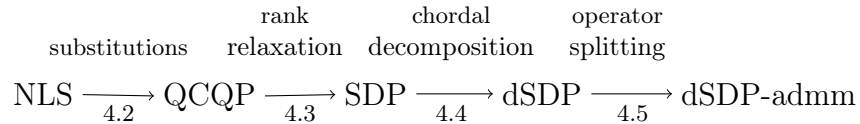
$$\min\{\text{tr}(\mathbf{Q}\mathbf{X}) \mid \mathbf{X} \succeq 0, \text{tr}(\mathbf{A}_i\mathbf{X}) = b_i, i = 1 \dots K\}, \quad (2)$$

where \mathbf{Q} is a symmetric cost matrix. Then we have the following property [58, Theorem 2.2]:

Theorem 1. *Let \mathcal{E}_{SDP} be the aggregate sparsity pattern of the set of problem matrices, $\{\mathbf{Q}, \mathbf{A}_1, \dots, \mathbf{A}_K\}$, and let \mathcal{G}_{SDP} be the sparsity graph corresponding to its chordal extension. Let the maximal cliques of \mathcal{G}_{SDP} be $\mathcal{C}_1, \dots, \mathcal{C}_T$ and let $\mathbf{C}_1, \dots, \mathbf{C}_T$ be the submatrices of \mathbf{X} at the indices of the cliques. Then we have: $\mathbf{X}_{\mathcal{E}} \succeq 0 \iff (\forall t) \mathbf{C}_t \succeq 0$.*

4 Method

In this section, we present two scalable methods for solving localization problems in robotics to global optimality, based on [58], which rely on the graph-theoretic concepts outlined in the previous section. We formally define the state estimation problem and its reformulation to a quadratically-constrained quadratic program (QCQP) in Sections 4.1 and 4.2, respectively. We then derive the monolithic SDP in 4.3 and show how it can be decomposed and distributed in Sections 4.4 and 4.5. A summarizing diagram of the different reformulations is given below.



4.1 Nonlinear least squares (NLS) formulation

Many classic state estimation problems in robotics, including localization and SLAM, take the form of a nonlinear least squares (NLS) problem when we seek the maximum a-posteriori estimator [5]:

$$\hat{\boldsymbol{\xi}} = \arg \min_{\boldsymbol{\xi} \in \mathcal{X}} \sum_{k \in \mathcal{Q}} \underbrace{\mathbf{e}_k(\boldsymbol{\xi}_k)^\top \mathbf{W}_k \mathbf{e}_k(\boldsymbol{\xi}_k)}_{a_k(\boldsymbol{\xi}_k)} + \sum_{(i,j) \in \mathcal{R}} \underbrace{\mathbf{e}_{ij}(\boldsymbol{\xi}_i, \boldsymbol{\xi}_j)^\top \mathbf{W}_{ij} \mathbf{e}_{ij}(\boldsymbol{\xi}_i, \boldsymbol{\xi}_j)}_{r_{ij}(\boldsymbol{\xi}_i, \boldsymbol{\xi}_j)}, \quad (3)$$

where $\boldsymbol{\xi} = \{\boldsymbol{\xi}_1, \dots, \boldsymbol{\xi}_N\}$ represents the poses or state variables to be estimated. We denote by $\mathcal{Q}(\mathcal{R})$ the set of indices (pairs) at which we have absolute (relative) measurements or prior terms. The absolute and relative cost terms are denoted $a_k(\boldsymbol{\xi}_k)$ and $r_{ij}(\boldsymbol{\xi}_i, \boldsymbol{\xi}_j)$, respectively, and defined by their respective error terms $\mathbf{e}(\cdot)$ and corresponding inverse covariance matrix \mathbf{W} .

Note that, for non-linear \mathbf{e}_k , \mathbf{e}_{ij} , or non-convex \mathcal{X} , Problem (3) may be non-convex and thus its globally optimal solution may be hard to find efficiently. Therefore, practitioners commonly resort to local solvers such as GN [5] or iSAM [29], which are efficient but have the important caveat that they may converge to poor local minima in the absence of a good initialization.

Factor-graph representation. Problem (3) can be represented by a factor graph $\mathcal{G}_f = (\mathcal{V}, \mathcal{M}, \mathcal{E})$ [18], where \mathcal{V} contains all states, \mathcal{M} contains the measurements or priors, and \mathcal{E} defines the (bipartite) connectivity between \mathcal{V} and \mathcal{M} . In this paper, we are interested in factor graphs that are chordally sparse – in other words, graphs that have small maximum cliques. One such example – where \mathcal{E} is a chain – is given in Figure 2. Throughout this paper, we will consider two localization problems as examples, which are exactly of the shown form.³ We define these problems next.

Example CT-RO. In continuous-time range-only localization (CT-RO), our goal is to find the position of a moving device over time, given distance measurements to N_m landmarks (also called anchors) of fixed and known locations. We are interested in the setup where the robot has only one tag and thus cannot estimate its orientation in the absence of additional modalities. Because distance measurements may be sparse, we add a Gaussian process (GP) motion prior to encourage smoothness and to ensure that recovery is possible even in underdetermined cases [6]. To ensure the Markovian property of the GP, we augment the state with temporal derivatives, depending on the type of motion prior being used. For conciseness, we focus on the constant-velocity motion prior in this paper, but the extension to other priors, such as constant-acceleration or zero-velocity, is straightforward [20]. Note that it was found in [20] that local solvers are prone to converge to local minima for this application, particularly when the landmarks are in degenerate configurations.

The state is given by $\boldsymbol{\xi}_i = \mathbf{x}_i = [\mathbf{t}_i^\top \mathbf{v}_i^\top]^\top$, where \mathbf{t}_i and \mathbf{v}_i are the position and velocity at time index i , respectively. The motion-prior errors are given by

³ Note that the decomposition method is not limited to chains, but chains are a particularly well-behaved structure with uniformly sized, small maximum cliques.

$\mathbf{e}_{ij} = \mathbf{x}_i - \Phi_{ij}\mathbf{x}_j$, where Φ_{ij} is the so-called transition matrix, and \mathbf{W}_{ij} is calculated using the GP motion-prior covariance [6]. Absolute measurements are given by $\mathbf{e}_k \in \mathbb{R}^{N_k}$ with N_k the number of landmarks seen at time index k , and the i -th element given by $\mathbf{e}_k[i] = \tilde{d}_{ki}^2 - \|\mathbf{t}_k - \mathbf{m}_i\|^2$, where \mathbf{m}_i is the i -th known landmark position, and \tilde{d}_{ki} is the corresponding distance measurement. The matrix \mathbf{W}_k is set to the assumed inverse covariance matrix of the squared distance measurements.

Example MW. In matrix-weighted localization (MW), we seek to estimate the pose of a moving device based on Euclidean observations of known landmarks. Because such observations typically come from sensors with varying accuracy in the radial and lateral directions, it is often crucial to allow for matrix-weighted, *i.e.*, anisotropic, measurement noise. It was found in [28] that this problem exhibits local minima, particularly as measurement anisotropy increases.

We have the following definitions: The state is defined by $\xi_i : \mathbf{T}_{i0} = \begin{bmatrix} \mathbf{C}_{i0} & \mathbf{t}_{0i}^i \\ \mathbf{0}^\top & 1 \end{bmatrix} \in SE(3)$, which transforms from the world frame (denoted by 0) to a local frame i , $\mathbf{C}_{i0} \in SO(3)$, and \mathbf{t}_{0i}^i is the translation from world to local frame i , expressed in local frame i . Given this state definition, the relative error terms can be expressed as $\mathbf{e}_{ij} = \text{vec}(\mathbf{T}_{i0} - \tilde{\mathbf{T}}_{ij}\mathbf{T}_{j0})$, where $\tilde{\mathbf{T}}_{ij}$ is a measurement of the relative transform from pose i to pose j . For relative measurements, we assume isotropic noise, thus $\mathbf{W}_{ij} = \sigma_{ij}^{-2}\mathbf{I}$. For absolute state measurements, we define $\mathbf{e}_{k,l} = \tilde{\mathbf{m}}_{lk}^k - \mathbf{T}_{k0}\mathbf{m}_{l0}^0$, where $\tilde{\mathbf{m}}_{lk}^k$ is the Euclidean measurement of landmark l as seen from pose k , and \mathbf{m}_{l0}^0 are the known landmark positions, expressed in world frame.

4.2 NLS to Quadratically Constrained Quadratic Program (QCQP)

In many applications of interest, Problem (3) can be written as a polynomial optimization problem, which can be formulated as an equivalent QCQP. The intuition is that we introduce a ‘lifted’ vector \mathbf{x} that contains ξ and potentially some higher-order ‘lifting functions’ thereof – enough so that both the cost and the constraints stemming from \mathcal{X} become quadratic in \mathbf{x} .

More specifically, we call the lifting functions $\ell_k(\xi_k)$ and introduce $h = 1$, the so-called ‘homogenization’ variable, which ensures that linear and constant cost terms can also be written in quadratic form. Introducing the vectors⁴

$$\mathbf{x}_k := [h \ \xi_k^\top \ \ell_k(\xi_k)^\top]^\top, \quad \mathbf{x}_{ij} := [h \ \xi_i^\top \ \ell_i(\xi_i)^\top \ \xi_j^\top \ \ell_j(\xi_j)^\top]^\top, \quad (4)$$

the QCQP reformulation of (3) takes the form:

$$\begin{aligned} \hat{\mathbf{x}} = \arg \min_{\mathbf{x}} \quad & \sum_k \mathbf{x}_k^\top \mathbf{Q}_k \mathbf{x}_k + \sum_{ij} \mathbf{x}_{ij}^\top \mathbf{R}_{ij} \mathbf{x}_{ij} \\ \text{s.t.} \quad & \mathbf{x}_k^\top \mathbf{A}_{jk}^s \mathbf{x}_k = b_{jk}, \quad k \in \mathcal{V}, j_k = 1 \dots N_k^s, \\ & \mathbf{x}_k^\top \mathbf{A}_{jk}^p \mathbf{x}_k = 0, \quad k \in \mathcal{V}, j_k = 1 \dots N_k^p \end{aligned} \quad (5)$$

⁴ We include one homogenization variable per variable group for simplicity of exposition. In practice, the homogenization variable can be shared among different groups.

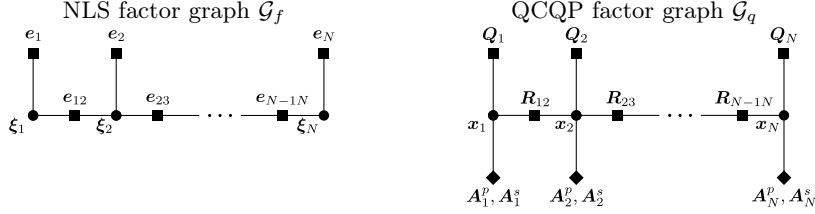


Fig. 2. Factor graphs [18] for the localization problems treated in this paper. On the left is the factor graph of the original NLS problem (3). On the right is a variant of factor graphs that we propose to describe the QCQP reformulation (5). This graph is formulated in terms of the lifted states \mathbf{x}_k and includes constraint and cost factors. Round nodes are variables, square nodes are cost terms, and diamonds are constraints.

where N_k^p is the number of primary constraints of node k (from \mathcal{X}) and N_k^s is the number of substitution constraints. The link between the cost matrices \mathbf{Q}_k and \mathbf{R}_{ij} and the original error terms in (3), as well as the form of the substitution and primary constraint matrices $\mathbf{A}_{jk}^s, \mathbf{A}_{ik}^p$, is given in Appendix A.1.

Factor-graph representation. We propose to represent the reformulated Problem (5) as a variant of factor graphs that includes constraints on variables in an analogous fashion to measurements, which has also been considered in [16, 44]. We call this factor graph \mathcal{G}_q and represent the new constraint factors with diamonds in Figure 2. The factor graph can be seen as the generalization of \mathcal{G}_f (which represents the cost of (3)) to the Lagrangian of (5). While there is a one-to-one mapping from the connectedness of the factor graph \mathcal{G}_f to the sparsity of the information matrix of the original problem (3) [18], the connectedness of the factor graph \mathcal{G}_q reflects the aggregate sparsity of the matrices \mathbf{Q} , \mathbf{A}_{jk}^s , and \mathbf{A}_{jk}^p in (5).

Examples. For brevity, we provide the details of the introduced lifting functions for the CT-RO and MW examples in Appendix A.2. The sparsity patterns of the problem matrices for the two examples are provided in Figure 3.

4.3 QCQP to Semidefinite Program (SDP)

We first derive the monolithic semidefinite relaxation of (5), which is our centralized baseline. To this end, we introduce the combined vector $\mathbf{x} \in \mathbb{R}^{N_x}$,

$$\mathbf{x} := [h \ \xi_1^\top \ \ell_1(\xi_1)^\top \ \cdots \ \xi_N^\top \ \ell_N(\xi_N)^\top]^\top, \quad (6)$$

and the projection matrices $\mathbf{E}^k, \mathbf{E}^{ij}$, defined implicitly through $\mathbf{x}_k = \mathbf{E}^k \mathbf{x}$, and $\mathbf{x}_{ij} = \mathbf{E}^{ij} \mathbf{x}$. Then, we rewrite (5) as

$$\begin{aligned} \hat{\mathbf{x}} &= \arg \min_{\mathbf{x}} \mathbf{x}^\top \mathbf{Q} \mathbf{x} + \mathbf{x}^\top \mathbf{R} \mathbf{x} \\ \text{s.t. } &\mathbf{x}^\top \bar{\mathbf{A}}_{jk}^s \mathbf{x} = b_{jk}, \quad k \in \mathcal{V}, j_k = 1 \dots N_k^s, \\ &\mathbf{x}^\top \bar{\mathbf{A}}_{jk}^p \mathbf{x} = 0, \quad k \in \mathcal{V}, j_k = 1 \dots N_k^p \end{aligned} \quad (7)$$

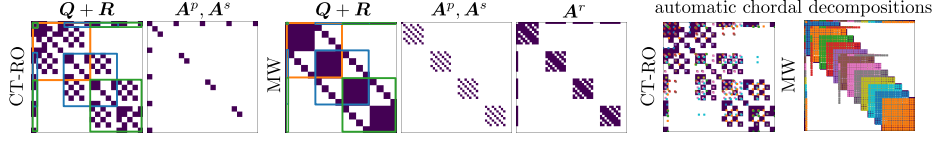


Fig. 3. Sparsity patterns for CT-RO and MW. We show the aggregate sparsity of the cost matrix $\mathbf{Q} + \mathbf{R}$, and the primary, substitution, and redundant constraints: \mathbf{A}^p , \mathbf{A}^s , and \mathbf{A}^r . The overlaid colored boxes on the cost matrix mark our used chordal decomposition of the aggregate sparsity patterns. The right-most plots show automatically generated chordal decompositions (different colors mark different cliques).

with $\mathbf{Q} = \sum_k \bar{\mathbf{Q}}_k$ and $\mathbf{R} = \sum_{ij} \bar{\mathbf{R}}_{ij}$. The constraint matrices, $\bar{\mathbf{A}}_{j_k}^p$, $\bar{\mathbf{A}}_{j_k}^s$, and the cost matrix $\bar{\mathbf{Q}}_k$ in (7), are obtained using $\bar{\mathbf{Y}}_k = \mathbf{E}^k \mathbf{Y}_k \mathbf{E}^{k\top}$. Similarly, we have defined $\bar{\mathbf{R}}_{ij} = \mathbf{E}^{ij} \mathbf{R}_{ij} \mathbf{E}^{ij\top}$.

Every QCQP can be relaxed to an SDP by using the succession of identities $\mathbf{x}^\top \mathbf{Q} \mathbf{x} = \text{tr}(\mathbf{x}^\top \mathbf{Q} \mathbf{x}) = \text{tr}(\mathbf{Q} \mathbf{x} \mathbf{x}^\top) = \{\text{tr}(\mathbf{Q} \mathbf{X}) | \mathbf{X} = \mathbf{x} \mathbf{x}^\top\} = \{\text{tr}(\mathbf{Q} \mathbf{X}) | \mathbf{X} \succeq 0, \text{rank } \mathbf{X} = 1\}$. By relaxing the rank-one constraint, we obtain the following primal relaxation of (7):

$$\begin{aligned} \hat{\mathbf{X}} &= \arg \min_{\mathbf{X} \succeq 0} \text{tr}(\mathbf{Q} \mathbf{X}) + \text{tr}(\mathbf{R} \mathbf{X}) \\ \text{s.t. } &\text{tr}(\bar{\mathbf{A}}_{j_k}^s \mathbf{X}) = b_{j_k}, \quad k \in \mathcal{V}, j_k = 1 \dots N_k^s, \\ &\text{tr}(\bar{\mathbf{A}}_{j_k}^p \mathbf{X}) = 0, \quad k \in \mathcal{V}, j_k = 1 \dots N_k^p, \\ &\text{tr}(\bar{\mathbf{A}}_i^r \mathbf{X}) = 0, \quad i = 1 \dots N_r \end{aligned} \quad (8)$$

where we have introduced $\bar{\mathbf{A}}_i^r$, so-called redundant constraints. Redundant constraints are trivially satisfied constraints of (7), *i.e.*, they are linearly dependent in (7) but are independent in (8). Their role is to help enforce the structure that may be lost when dropping the rank constraint, thus encouraging the solution $\hat{\mathbf{X}}$ to be of low rank. This is important because only if the optimal solution $\hat{\mathbf{X}}$ of (8) is of rank one can we obtain the globally optimal solution $\hat{\mathbf{x}}$ of (7) from the factorization $\hat{\mathbf{X}} = \hat{\mathbf{x}} \hat{\mathbf{x}}^\top$ (in which case we say that the relaxation is *tight*).

We end this section by making a few observations about the process of relaxing (3) to the SDP (8). Problem (8) is a convex problem that can be solved to global optimality in polynomial time, but a naive application of off-the-shelf solvers would lead to approximately cubic complexity. Indeed, the constraint $\mathbf{X} \succeq 0$ somewhat breaks the sparsity of the graph \mathcal{G}_q as it implicitly adds edges between all variables. However, Theorem 1 suggests that if the measurement graph \mathcal{G}_p is chordally sparse, we can regain efficiency by splitting the problem into its maximal cliques. Note that the redundant constraints $\bar{\mathbf{A}}_i^r$, which may be required for tightness, can also induce new dependencies in \mathcal{G}_p and reduce sparsity (*i.e.*, increase the size of the maximal cliques). Thus, we deal with opposing forces: without redundant constraints, the SDP relaxation may not be tight, preventing us from getting a globally optimal estimate. However, adding redundant constraints may reduce sparsity and prevent us from effectively solving the SDP.

As we see next, the two example problems have tight semidefinite relaxations with essentially unchanged sparsity patterns.

Example CT-RO. For this example problem, the relaxation is already tight without the need for redundant constraints, as observed in [20] and [19].

Example MW. For this problem, we can add the following well-known redundant constraints [10]: $\text{vech}(\mathbf{C}_{i0})^\top \text{vech}(\mathbf{C}_{i0}^\top) = \text{vech}(\mathbf{I}_3)^5$ and the redundant handedness constraints $\mathbf{C}_{i0}[2] \times \mathbf{C}_{i0}[3] = \mathbf{C}_{i0}[1]$ and $\mathbf{C}_{i0}[3] \times \mathbf{C}_{i0}[1] = \mathbf{C}_{i0}[2]$. It was shown in [28] that these redundant constraints may significantly improve tightness as the noise level increases and the number of measurements decreases. Since the constraints depend only on one pose at a time, they do not change the structure of the measurement graph, which can also be observed from the sparsity patterns in Figure 3.

4.4 Decomposed solution: dSDP

We can now describe our monolithic solver, which decomposes the problem into smaller parts but runs in a centralized way. We adopt a vectorized SDP formulation from here on for notational convenience. In particular, we introduce variable $\mathbf{y} = \text{vech}(\mathbf{X})$ and $\mathbf{y}_k = \text{vech}(\mathbf{X}_k)$. Using this notation, we can write (8) in the standard dual form for conic programs [9]:

$$\begin{aligned} \hat{\mathbf{y}} = \arg \min_{\mathbf{y} \succeq 0} \quad & \sum_{k \in \mathcal{Q}} \tilde{\mathbf{q}}_k^\top \mathbf{y}_k + \sum_{i,j \in \mathcal{R}} \tilde{\mathbf{r}}_{ij}^\top \mathbf{y}_{ij}, \\ \text{s.t. } \quad & \mathbf{A}_n \mathbf{y}_n = \mathbf{b}_n, \quad n \in \mathcal{V} \end{aligned} \quad (9)$$

where we have introduced $\tilde{\mathbf{q}}_k := \text{vech}(\mathbf{Q}_k)$, $\tilde{\mathbf{r}}_{ij} := \text{vech}(\mathbf{R}_{ij})$, and we have grouped all primary, substitution, and redundant constraints into \mathbf{A}_n :

$$\mathbf{A}_n^\top := [\cdots \text{vech}(\mathbf{A}_{j_k}^p) \cdots \text{vech}(\mathbf{A}_{j_k}^s) \cdots \text{vech}(\mathbf{A}_{j_k}^r) \cdots], \quad (10)$$

and \mathbf{b}_n is defined accordingly. Typically, the lack of speed in SDPs is due to the semidefinite constraint on \mathbf{y} . However, we are now in a position to apply Theorem 1, which will allow us to decompose this constraint into a sequence of smaller positive-definiteness constraints. Indeed, if the aggregate sparsity pattern of the SDP is chordally sparse, we can replace the condition $\mathbf{y} \succeq 0$ with $\mathbf{c}_t \succeq 0$, $t = 1 \dots T$ where \mathbf{c}_t correspond to the variables from the clique t .

Given the aggregate sparsity pattern of Problem (8), we could automatically compute the maximal cliques using efficient heuristics [54]. Figure 3, on the right, gives example decompositions using the approximate minimum degree ordering. We observe that the method has generated some fill-in between variables groups that do not have dependencies in the original graph \mathcal{G}_q . This reduces the sparsity, which would affect our solver's computational cost. Instead, we suggest using a manual decomposition, which, although potentially less minimal, avoids such dependencies and generates fewer cliques. Indeed, a straightforward decomposition

⁵ We use only 5 of these 6 constraints since one is linearly dependent.

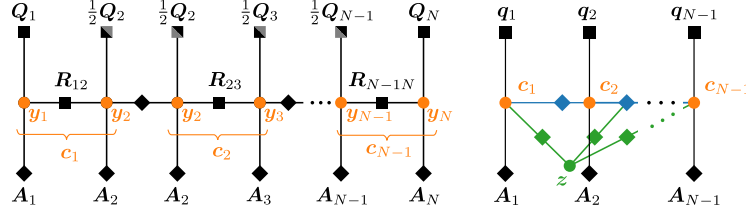


Fig. 4. Visualization of the decomposition of the chordal localization problems. On the left is the factor graph split into maximal cliques, with the shared cost terms $Q_i, i = 1 \dots N-1$ split into half, and constraints added to enforce the overlap of neighboring cliques. On the right is the corresponding clique tree, used for dSDP (constraints in blue) and dSDP-admm (consensus variable z and constraints shown in green).

of the problem is given by $\mathbf{c}_i = (h, \mathbf{y}_i, \mathbf{y}_{i+1})$, shown also in Figure 3 for the same example. For simplicity, we use the trivial maximal chordal extension within each clique: the clique completion, and do not exploit the aggregate sparsity within each clique. This would be expected to only lead to minor improvement and is left for future work.⁶

More formally, we define the *chordal clique tree* $\mathcal{T}_c := (\mathcal{V}_c, \mathcal{E}_c)$, whose vertices index the cliques including the associated cost and constraint terms, and edges between two cliques indicate that they share variables. This is necessarily a tree because any loop closure in this graph would violate the definition of maximal cliques. Using this notion and Theorem 1 we can define the (dSDP) problem:

$$\begin{aligned} \{\hat{\mathbf{c}}_1, \dots, \hat{\mathbf{c}}_T\} = \arg \min_{\mathbf{c}_1, \dots, \mathbf{c}_T} \sum_{t \in \mathcal{V}_c} \mathbf{q}_t^\top \mathbf{c}_t \\ \text{s.t. } \mathbf{A}_t \mathbf{c}_t = \mathbf{b}_t, \quad t \in \mathcal{V}_c, \\ \mathbf{E}_t^{t'} \mathbf{c}_t = \mathbf{E}_{t'}^t \mathbf{c}_{t'}, \quad t, t' \in \mathcal{E}_c \\ \mathbf{c}_t \succeq 0, \quad t \in \mathcal{V}_c \end{aligned} \quad (11)$$

where $\mathbf{E}_t^{t'}$ is the indexing matrix selecting the shared variables with t' from clique t , and \mathbf{q}_t is the clique-wise cost vector, obtained from:

$$\mathbf{q}_t := \sum_{k \in \mathcal{C}_t} \frac{1}{N_k} \text{vech}(\mathbf{E}_t^{k\top} \mathbf{Q}_k \mathbf{E}_t^k) + \sum_{i,j \in \mathcal{C}_t} \frac{1}{N_{ij}} \text{vech}(\mathbf{E}_t^{ij\top} \mathbf{R}_{ij} \mathbf{E}_t^{ij}), \quad (12)$$

where N_k, N_{ij} are the numbers of occurrences of node k or edge (i, j) , respectively, in graph \mathcal{G}_q . Equation (12) equally splits cost terms among overlapping nodes, making sure that the total cost is preserved. Problem (11) can be solved by any off-the-shelf SDP solver.

Factor-graph representation. The process of splitting variables and associated cost terms is visualized, for our example problems, in the factor graph

⁶ This manual decomposition also works for graphs that are not simple chains: we can first find a chordal decomposition at the variable block level and then use the maximal chordal extension within each block.

in Figure 4 (a). We also provide a sketch of the associated clique tree, which includes the introduced overlap constraints in (11). Note that the proposed decomposition has the advantage of having a clean factor-graph representation since it keeps the original variable groups intact.

Problem (11) has the potential of being significantly faster to solve because the large SDP variable is split into T smaller ones. As the complexity of interior-point solvers depends on both the problem dimension and the number of constraints [1], the speedup is a function of the number of cliques, their size, and their connectivity. We will see that this speed-up is significant for the studied localization problems and our manual decomposition. Note that the problem is still solved in a centralized manner as the overlapping constraints introduce dependencies between the cliques. Next, we formulate the distributed algorithm.

4.5 Distributed solution: dSDP-admm

In this section, we state a distributed version of dSDP using ADMM, which we call dSDP-admm. In general, ADMM solves problems of the form [8]:

$$\begin{aligned} \min_{\mathbf{c}, \mathbf{z}} \quad & f(\mathbf{c}) + g(\mathbf{z}) \\ \text{s.t.} \quad & \mathbf{A}\mathbf{c} + \mathbf{B}\mathbf{z} = \mathbf{0} \end{aligned} \quad (13)$$

The ADMM algorithm has proven convergence guarantees even when f and g are not necessarily smooth, which we will exploit to incorporate non-linear constraints through the use of indicator functions.

Our method is an adaptation of the so-called consensus ADMM [8, Chapter 7], where one variable group contains local but overlapping variables, and the other variable group contains the ‘consensus’ among overlapping variables. To see this, we create the feasible set $\mathcal{F}_t := \{\mathbf{c}_t | \mathbf{c}_t \succeq 0, \mathbf{A}_t \mathbf{c}_t = \mathbf{b}_t\}$ and define the indicator function $\mathcal{I}_{\mathcal{F}_t}(\mathbf{x})$ which maps to 0 when $\mathbf{x} \in \mathcal{F}_t$ and to ∞ otherwise. Then, we can reformulate (11) as follows:

$$\begin{aligned} \min_{\mathbf{c}_t} \quad & \sum_{t \in \mathcal{V}_c} \mathbf{q}_t^\top \mathbf{c}_t + \mathcal{I}_{\mathcal{F}_t}(\mathbf{c}_t) \\ \text{s.t.} \quad & \mathbf{E}^t \mathbf{z} = \mathbf{c}_t, \quad t \in \mathcal{V}_c \end{aligned} \quad (14)$$

where we have introduced the consensus variable \mathbf{z} , similar to \mathbf{x} in the original problem. Importantly, the semi-definite constraint is now on the smaller variables \mathbf{c}_t . The clique tree corresponding to this problem is shown in Figure 4(b).

Applying the standard ADMM iterations to (14), we get:

$$\mathbf{c}^i = \arg \min_{\mathbf{c}} \mathcal{L}_\rho(\mathbf{c}, \mathbf{z}^i, \boldsymbol{\lambda}^i), \quad (15a)$$

$$\mathbf{z}^i = \arg \min_{\mathbf{z}} \mathcal{L}_\rho(\mathbf{c}^i, \mathbf{z}, \boldsymbol{\lambda}^i), \quad (15b)$$

$$(\forall t) : \boldsymbol{\lambda}_t^{i+1} = \boldsymbol{\lambda}_t^i + \rho (\mathbf{E}^t \mathbf{z}^i - \mathbf{c}_t^i), \quad (15c)$$

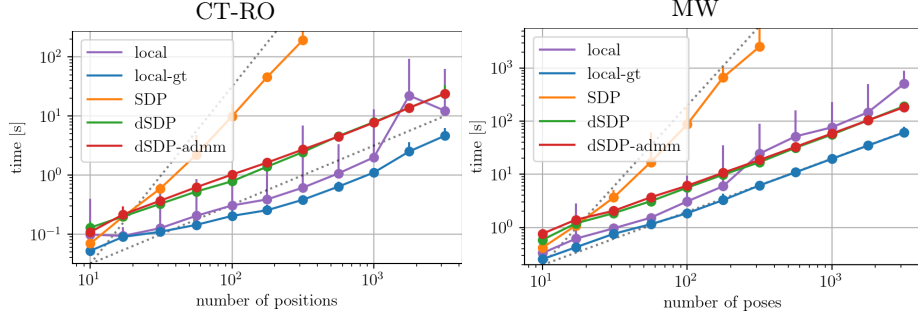


Fig. 5. Solver times for increasing problem sizes for range-only localization (left) and matrix-weighted localization (right). The dashed gray lines correspond to $O(N)$ and $O(N^3)$. The presented sparsity-exploiting algorithms have a complexity comparable with the local solver and with little variance. On average, the local solver is faster than the decomposed methods but has a high variance (vertical bars) depending on the initialization.

where the augmented Lagrangian is given by $\mathcal{L}_\rho(\mathbf{c}, \mathbf{z}, \boldsymbol{\lambda}) = f(\mathbf{c}_1) + g(\mathbf{z}) + \boldsymbol{\lambda}^\top (\mathbf{E}^t \mathbf{z}^i - \mathbf{c}_t) + \frac{\rho}{2} \|\mathbf{E}^t \mathbf{z}^i - \mathbf{c}_t\|^2$. Thanks to the introduction of \mathbf{z} , step (15a) can now be decomposed into T optimization problems, each of which is a SDP with quadratic cost that can be reformulated to a linear SDP using a linear matrix inequality, see *e.g.*, [34].

The second step (15b) is an unconstrained problem and has a closed-form solution. The solution is very intuitive: each element of \mathbf{z} , consists of the average of the corresponding clique values. Therefore, \mathbf{z} can also be updated in a distributed manner, where current values of \mathbf{c}^i need to be shared only between overlapping cliques. Because (15c) is distributed by definition, the entire algorithm can be run in a distributed fashion.

5 Localization Results

We test the two methods in simulation on the two example localization problems, evaluating their performance in terms of efficiency, optimality, and accuracy, compared with local and standard SDP solvers.

5.1 Setup

We generate example problems in simulation as follows.

Example CT-RO. We draw N_m landmarks uniformly at random from a cube of dimension 10 m, emulating the setup of anchors such as ultra-wideband tags inside an arena. Then, within the same cube, we generate a random trajectory of N states at times sampled uniformly at random and sorted from 0 to $N - 1$. We use the constant-velocity motion prior [6, Section IV.A] with random initial velocity of 0.1 ms^{-1} and standard deviation (STD) $\sigma_a = 0.2 \text{ ms}^{-2}$, making sure the trajectory stays within the cube. Then, we simulate distance measurements

by adding i.i.d Gaussian noise of STD $\sigma_d = 10$ cm, unless stated otherwise, to each squared distance. We set the prior distance measurement noise to $\check{\sigma}_d = 1$ mm and $\check{\sigma}_a = 0.2 \text{ ms}^{-2}$, set $\mathbf{W}_k = \check{\sigma}_d^{-2} \mathbf{I}_{N_k}$ and form \mathbf{W}_{ij} according to the GP prior, as explained in [6].

Example MW. We generate N_m landmarks uniformly at random from a cube of dimension 1 m centered at the origin, emulating visual features in a given area. Then, we sample random poses uniformly at random with coordinates \mathbf{t}_{i0}^0 in $(-0.1 \text{ m}, -0.1 \text{ m}, 2.9 \text{ m})$, $(0.1 \text{ m}, 0.1 \text{ m}, 3.1 \text{ m})$, with the z -axis pointing downwards with randomly generated yaw angles between 0 and 2π . We use camera parameters $f = 1077$, $c = 0$, $b = 0.12 \text{ mm}$ and pixel standard deviation $\sigma_u = \sigma_v = 1.0$, unless stated otherwise. We generate pixel and non-isotropic \mathbf{W}_k from these parameters by linearizing the pinhole measurement model as explained in [28]. Similarly, we generate relative motion measurements and \mathbf{W}_{ij} with translation STD $\sigma_t = 1$ cm and rotation STD $\sigma_r = 10$ deg.

We solve one example per problem size for the timing studies, while for the noise study, we average over 10 random problem instances. For all SDP solvers, we use the *MOSEK Fusion API for Python* [2], and we set one global tolerance parameter τ per algorithm. τ is used to update the primal feasibility, dual feasibility, and relative duality gap parameters. For dSDP and SDP, we use $\tau^{\text{dSDP}} = \tau^{\text{SDP}} = 10^{-10}$. For the local solvers, we use our custom GN implementations with the stopping criterion that the element-wise maximum of the gradient is below $\tau^{\text{GN}} = 10^{-7}$ or at a number of iterations above $N_{\text{it}}^{\text{GN}} = 100$. We consider random initializations of GN, drawn randomly from a Gaussian of standard deviation 0.5 around the ground truth (*local*), and initializing at ground truth (*local-gt*).

For dSDP-admm, we use the penalty adaptation rule described in [8, eq. (3.13)], with $\mu = 10$ and $\tau = 2.0$. For the convergence criteria, we use thresholds on the two-norms of the primal and dual residuals as suggested in [8, eq. (3.12)], where we use only the relative criterion to calculate the threshold with $\epsilon^{\text{rel}} = 10^{-10}$ or maximum number iterations $N_{\text{it}}^{\text{dSDP-admm}} = 10$. Because dSDP-admm does not require its inner iterations to be very precise, we set the tolerance $\tau^{\text{dSDP-admm}}$ for the inner SDP to 10^{-3} . We run all algorithms on a server with 2 *Intel Xeon* processors, giving 24 physical cores and 48 threads, and equipped with 320 GB of RAM.

5.2 Efficiency

First, we investigate the speed of the proposed methods as a function of the problem size. Figure 5 shows the performance of the two proposed algorithms as a function of the number of poses or positions. We observe that the decomposed methods are significantly faster than the full SDP method. In fact, these decomposed methods are competitive with the local GN solver (same runtime complexity) yet can still provide a certified globally optimal solution.

Due to hardware limitations and communication overhead, the optimal number of threads for dSDP-admm is fixed to 10, and is run for a fixed number of

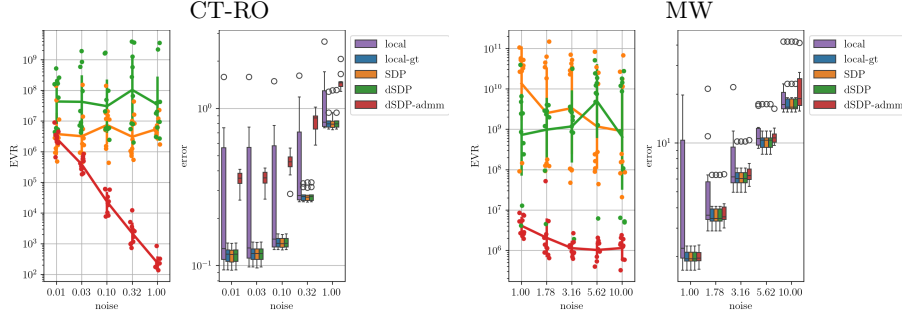


Fig. 6. Tightness and accuracy studies for increasing noise levels for range-only localization (left) and matrix-weighted localization (right). Noise is added to the squared distance measurements (in meters) and pixel observations. All results are with $N = 100$ and $N_m = 8$.

iterations 3. We expect the performance of dSDP-admm to improve as more computational nodes are available.

5.3 Optimality

Next, we investigate the tightness of our relaxations with respect to the noise level. To this end, we compute the eigenvalue ratio $\text{EVR} = \lambda_0/\lambda_1$ with λ_i the eigenvalues of the solution of the relaxation \mathbf{X}^* , in decreasing order. This ratio measures how close the solution is to being rank one.

Looking at the Eigenvalue ratio (EVR) in Figure 6, we observe that the relaxation becomes less tight with increasing noise levels, as expected. For CT-RO in particular, the fact that we terminate dSDP-admm after a fixed number of iterations means that the solution quality deteriorates as the noise increases. We argue that this is due to a looser connection between nodes; consisting only of a motion prior as opposed to pose-to-pose measurements. It may thus be harder for the alternating algorithm to reach ‘consensus’; for higher noise levels, the different subproblems pull in different directions at each iteration. Here, we see a fundamental speed *vs.* accuracy trade when using the ADMM algorithm. In this example, we have opted for speed, but we can see that increased noise causes the ADMM algorithm to struggle to yield accurate results. The SDP and dSDP algorithms, on the other hand, reach consistently high EVR for all noise levels for CT-RO.

For MW, we observe that adding redundant constraints significantly affects the tightness of the relaxation and renders the EVR almost constant for all considered noise levels. The added computational cost for achieving higher tightness is minimal, as can be observed in Figure 5. We observe again that dSDP-admm is significantly less tight than the other algorithms but still achieves high enough EVR to suggest a rank-one solution.

5.4 Accuracy

Finally, the accuracy of the algorithms is measured in terms of the distance between ground truth values and estimates. We choose the Euclidean distance for vector-valued functions and the chordal distance for rotation estimates. The accuracy obtained by the different solvers is reported in Figure 6. We observe that the randomly initialized local solver (*local*) has a high variance because it converges to local minima. The *local-gt* solver, SDP, and dSDP, on the other hand, solve the problem to almost identical accuracy. Only dSDP-admm has a significantly worse accuracy, particularly for the CT-RO example, because it would require more than the imposed three iterations to converge. This emphasizes the typical trade-off between accuracy and runtime present for dSDP-admm. With an improved implementation of dSDP-admm⁷, the method could be distributed more effectively and could run with higher accuracy without compromising speed.

6 Conclusion and Future Work

We have shown that a large class of optimization problems that typically occur in robotics allow for linear-time SDP solvers using the chordal decomposition of the underlying aggregate sparsity graph. This decomposition can be used to speed up centralized computation but also lends itself to an ADMM-based distributed implementation, which we also tested. Most importantly, the methods are on par with efficient local solvers in terms of computational complexity, but with the great advantage that they are global solvers for reasonable noise levels and thus cannot converge to poor local minima.

Possible improvements include the adoption of known heuristics for speeding up our vanilla ADMM, such as diagonal rescaling for better conditioning [25], or the use of a fast approximate interior-point solver [46]. The behavior of the algorithms when the problem is not chordally sparse presents another interesting direction of research, with possible extensions of the algorithms including the factor-width decomposition [58], loopy belief propagation [40], or using the chordal reduction as an initialization technique for more exact solvers.

Acknowledgments. FD is funded by the ANR JCJC project NIMBLE (ANR-22-CE33-0008). Most of this work was conducted while FD was with the University of Toronto, funded by the Swiss National Science Foundation, Postdoc Mobility under Grant 206954. The Natural Sciences and Engineering Research Council of Canada (NSERC) also partly funded this work.

Disclosure of Interests. The authors have no competing interests to declare that are relevant to the content of this article.

⁷ The current implementation uses Python, which does not allow for effective multi-threading.

References

1. Andersen, E., Roos, C., Terlaky, T.: On implementing a primal-dual interior-point method for conic quadratic optimization. *Mathematical Programming* **95**(2), 249–277 (2003), <http://link.springer.com/10.1007/s10107-002-0349-3>
2. Aps, M.: The MOSEK Fusion API for Python 10.1.22. Tech. rep. (2024), <https://docs.mosek.com/latest/pythonfusion/index.html>
3. Bambade, A., El-Kazdadi, S., Taylor, A., Carpentier, J.: PROX-QP: Yet another Quadratic Programming Solver for Robotics and beyond. In: *Robotics: Science and Systems* (2022), <http://www.roboticsproceedings.org/rss18/p040.pdf>
4. Bambade, A., Schramm, F., Kazdadi, S.E., Caron, S., Taylor, A., Carpentier, J.: PROXQP: An Efficient and Versatile Quadratic Programming Solver for Real-Time Robotics Applications and Beyond. hal-04198663v2 (2023), <https://inria.hal.science/hal-04198663>
5. Barfoot, T.D.: *State Estimation for Robotics*. Cambridge University Press (2017), <https://www.cambridge.org/core/product/identifier/9781316671528/type/book>
6. Barfoot, T.D., Hay Tong, C., Särkkä, S.: Batch continuous-time trajectory estimation as exactly sparse Gaussian process regression. In: *Robotics: Science and Systems* (2014), <http://www.roboticsproceedings.org/rss10/p01.pdf>
7. Barfoot, T.D., Holmes, C., Dümbgen, F.: Certifiably Optimal Rotation and Pose Estimation Based on the Cayley Map. arXiv:2308.12418 [cs] (2023), arxiv.org/abs/2308.12418
8. Boyd, S.: Distributed Optimization and Statistical Learning via the Alternating Direction Method of Multipliers. *Foundations and Trends in Machine Learning* **3**(1), 1–122 (2010), <http://www.nowpublishers.com/article/Details/MAL-016>
9. Boyd, S., Vandenberghe, L.: *Convex Optimization*. Cambridge University Press (2004), <https://web.stanford.edu/~boyd/cvxbook/>
10. Briales, J., Gonzalez-Jimenez, J.: Convex Global 3D Registration with Lagrangian Duality. In: *IEEE/CVF Conference on Computer Vision and Pattern Recognition (CVPR)*. pp. 5612–5621 (2017), <http://ieeexplore.ieee.org/document/8100078/>
11. Carlone, L., Calafiore, G.C., Tommolillo, C., Dellaert, F.: Planar Pose Graph Optimization: Duality, Optimal Solutions, and Verification. *IEEE Transactions on Robotics* **32**(3), 545–565 (2016), <https://doi.org/10.1109/TR0.2016.2544304>
12. Carlone, L., Kaouk Ng, M., Du, J., Bona, B., Indri, M.: Simultaneous Localization and Mapping Using Rao-Blackwellized Particle Filters in Multi Robot Systems. *Journal of Intelligent & Robotic Systems* **63**(2), 283–307 (2011), <http://link.springer.com/10.1007/s10846-010-9457-0>
13. Choudhary, S., Carlone, L., Nieto, C., Rogers, J., Christensen, H.I., Dellaert, F.: Distributed mapping with privacy and communication constraints: Lightweight algorithms and object-based models. *The International Journal of Robotics Research* **36**(12), 1286–1311 (2017), <http://journals.sagepub.com/doi/10.1177/0278364917732640>
14. Cieslewski, T., Choudhary, S., Scaramuzza, D.: Data-Efficient Decentralized Visual SLAM. In: *IEEE International Conference on Robotics and Automation (ICRA)*. pp. 2466–2473 (2018), <https://ieeexplore.ieee.org/document/8461155/>
15. Cohn, T., Petersen, M., Simchowitz, M., Tedrake, R.: Non-Euclidean Motion Planning with Graphs of Geodesically-Convex Sets. In: *Robotics: Science and Systems* (2023), <http://www.roboticsproceedings.org/rss19/p057.pdf>

16. Cunningham, A., Paluri, M., Dellaert, F.: DDF-SAM: Fully distributed SLAM using Constrained Factor Graphs. In: IEEE/RSJ International Conference on Intelligent Robots and Systems. pp. 3025–3030 (2010), <https://ieeexplore.ieee.org/document/5652875>
17. Dall’Anese, E., Zhu, H., Giannakis, G.B.: Distributed Optimal Power Flow for Smart Microgrids. IEEE Transactions on Smart Grid **4**(3), 1464–1475 (2013), <https://ieeexplore.ieee.org/document/6502290/>
18. Dellaert, F.: Factor graphs : Exploiting structure in robotics. Annual Review of Control, Robotics and Autonomous Systems **4**, 141–166 (2021), <https://www.annualreviews.org/doi/10.1146/annurev-control-061520-010504>
19. Dümbsen, F., Holmes, C., Agro, B., Barfoot, T.D.: Toward Globally Optimal State Estimation Using Automatically Tightened Semidefinite Relaxations. arXiv:2308.05783 [cs] (2023), <https://doi.org/10.48550/arXiv.2308.05783>
20. Dümbsen, F., Holmes, C., Barfoot, T.D.: Safe and Smooth: Certified Continuous-Time Range-Only Localization. IEEE Robotics and Automation Letters **8**(2), 1117–1124 (2023), <https://doi.org/10.1109/LRA.2022.3233232>
21. Eriksson, A., Olsson, C., Kahl, F., Chin, T.J.: Rotation averaging and strong duality. In: IEEE/CVF Conference on Computer Vision and Pattern Recognition (CVPR). pp. 127–135 (2018), <https://doi.org/10.1109/CVPR.2018.00021>
22. Fan, T., Ortiz, J., Hsiao, M., Monge, M., Dong, J., Murphey, T., Mukadam, M.: Decentralization and Acceleration Enables Large-Scale Bundle Adjustment. In: Robotics: Science and Systems (2022), <http://arxiv.org/abs/2305.07026>
23. Fredriksson, J., Olsson, C.: Simultaneous multiple rotation averaging using lagrangian duality. In: Asian Conference on Computer Vision. pp. 245–258 (2013), http://link.springer.com/10.1007/978-3-642-37431-9_19
24. Fukuda, M., Kojima, M., Murota, K., Nakata, K.: Exploiting Sparsity in Semidefinite Programming via Matrix Completion I: General Framework. SIAM Journal on Optimization **11**(3), 647–674 (2001), <https://epubs.siam.org/doi/10.1137/S1052623400366218>
25. Giselsson, P., Boyd, S.: Diagonal scaling in Douglas-Rachford splitting and ADMM. In: IEEE Conference on Decision and Control (CDC). pp. 5033–5039 (2014), <https://ieeexplore.ieee.org/abstract/document/7040175>
26. Goudar, A., Dümbsen, F., Barfoot, T.D., Schoellig, A.P.: Optimal Initialization Strategies for Range-Only Trajectory Estimation. IEEE Robotics and Automation Letters **9**(3), 2160–2167 (2024), <https://ieeexplore.ieee.org/document/10400824>
27. Holmes, C., Barfoot, T.D.: An Efficient Global Optimality Certificate for Landmark-Based SLAM. IEEE Robotics and Automation Letters **8**(3), 1539–1546 (2023), <https://ieeexplore.ieee.org/document/10023976>
28. Holmes, C., Dümbsen, F., Barfoot, T.D.: On Semidefinite Relaxations for Matrix-Weighted State-Estimation Problems in Robotics. arXiv:2308.07275 [cs, math] (2023), <http://arxiv.org/abs/2308.07275>
29. Kaess, M., Ranganathan, A., Dellaert, F.: iSAM: Incremental Smoothing and Mapping. IEEE Transactions on Robotics **24**(6), 1365–1378 (2008), <http://ieeexplore.ieee.org/document/4682731/>
30. Kaess, M., Johannsson, H., Roberts, R., Ila, V., Leonard, J.J., Dellaert, F.: iSAM2: Incremental smoothing and mapping using the bayes tree. International Journal of Robotics Research **31**(2), 216–235 (2012), <https://doi.org/10.1177/0278364911430419>

31. Kahl, F., Henrion, D.: Globally Optimal Estimates for Geometric Reconstruction Problems. *International Journal of Computer Vision* **74**(1), 3–15 (2007), <https://link.springer.com/10.1007/s11263-006-0015-y>
32. Kalbat, A., Lavaei, J.: A fast distributed algorithm for decomposable semidefinite programs. In: *IEEE Conference on Decision and Control (CDC)*. pp. 1742–1749 (2015), <http://ieeexplore.ieee.org/document/7402462/>
33. Kim, S., Kojima, M., Mevisen, M., Yamashita, M.: Exploiting sparsity in linear and nonlinear matrix inequalities via positive semidefinite matrix completion. *Mathematical Programming* **129**(1), 33–68 (2011), <http://link.springer.com/10.1007/s10107-010-0402-6>
34. Madani, R., Kalbat, A., Lavaei, J.: ADMM for sparse semidefinite programming with applications to optimal power flow problem. In: *IEEE Conference on Decision and Control (CDC)*. pp. 5932–5939 (2015), <http://ieeexplore.ieee.org/document/7403152/>
35. Marcucci, T., Petersen, M., von Wrangel, D., Tedrake, R.: Motion Planning around Obstacles with Convex Optimization. *arXiv:2205.04422 [cs]* (2022), <https://doi.org/10.48550/arXiv.2205.04422>
36. Murai, R., Alzugaray, I., Kelly, P.H., Davison, A.J.: Distributed Simultaneous Localisation and Auto-Calibration Using Gaussian Belief Propagation. *IEEE Robotics and Automation Letters* **9**(3), 2136–2143 (2024), <https://ieeexplore.ieee.org/document/10387679/>
37. Nocedal, J., Wright, S.J.: *Numerical Optimization*. Springer Series in Operation Research, Springer-Verlag, New York, NY, 2nd edition edn. (2006), <https://link.springer.com/book/10.1007/978-0-387-40065-5>
38. O’Donoghue, B., Chu, E., Parikh, N., Boyd, S.: Conic Optimization via Operator Splitting and Homogeneous Self-Dual Embedding. *Journal of Optimization Theory and Applications* **169**(3), 1042–1068 (2016), <https://doi.org/10.1007/s10957-016-0892-3>
39. Olsson, C., Kahl, F., Oskarsson, M.: Branch-and-Bound Methods for Euclidean Registration Problems. *IEEE Transactions on Pattern Analysis and Machine Intelligence* **31**(5), 783–794 (2009), <https://doi.org/10.1109/TPAMI.2008.131>
40. Ortiz, J., Evans, T., Davison, A.J.: A visual introduction to Gaussian Belief Propagation. <http://arxiv.org/abs/2107.02308> (2021)
41. Ortiz, J., Pupilli, M., Leutenegger, S., Davison, A.J.: Bundle Adjustment on a Graph Processor. In: *IEEE/CVF Conference on Computer Vision and Pattern Recognition (CVPR)*. pp. 2413–2422. Seattle, WA, USA (2020), <https://ieeexplore.ieee.org/document/9157499/>
42. Papalia, A., Fishberg, A., O’Neill, B.W., How, J.P., Rosen, D.M., Leonard, J.J.: Certifiably Correct Range-Aided SLAM. *arXiv:2302.11614 [cs]* (2023), <https://doi.org/10.48550/arXiv.2302.11614>
43. Parra, Á., Chng, S.F., Chin, T.J., Eriksson, A., Reid, I.: Rotation Coordinate Descent for Fast Globally Optimal Rotation Averaging. In: *IEEE/CVF Conference on Computer Vision and Pattern Recognition (CVPR)*. pp. 4296–4305 (2021), <https://doi.org/10.1109/CVPR46437.2021.00428>
44. Qadri, M., Sodhi, P., Mangelson, J.G., Dellaert, F., Kaess, M.: InCOpt: Incremental Constrained Optimization using the Bayes Tree. In: *IEEE/RSJ International Conference on Intelligent Robots and Systems (IROS)*. pp. 6381–6388 (2022), <https://ieeexplore.ieee.org/document/9982178/>
45. Rawlings, J.B., Mayne, D.Q., Diehl, M.: *Model Predictive Control: Theory, Computation, and Design*. Nob Hill Publishing, Santa Barbara, California, 2nd edition

- edn. (2020)
46. Rontsis, N., Goulart, P., Nakatsukasa, Y.: Efficient Semidefinite Programming with Approximate ADMM. *Journal of Optimization Theory and Applications* **192**(1), 292–320 (2022), <https://doi.org/10.1007/s10957-021-01971-3>
 47. Rosen, D.M., Carlone, L., Bandeira, A.S., Leonard, J.J.: SE-sync: A certifiably correct algorithm for synchronization over the special euclidean group. *International Journal of Robotics Research* **38**(2-3), 95–125 (2019), <http://journals.sagepub.com/doi/10.1177/0278364918784361>
 48. Shi, W., Ling, Q., Yuan, K., Wu, G., Yin, W.: On the Linear Convergence of the ADMM in Decentralized Consensus Optimization. *IEEE Transactions on Signal Processing* **62**(7), 1750–1761 (Apr 2014), <http://arxiv.org/abs/1307.5561>
 49. Stellato, B., Banjac, G., Goulart, P., Bemporad, A., Boyd, S.: OSQP: An operator splitting solver for quadratic programs. *Mathematical Programming Computation* **12**(4), 637–672 (2020), <http://link.springer.com/10.1007/s12532-020-00179-2>
 50. Sun, Y., Andersen, M.S., Vandenberghe, L.: Decomposition in Conic Optimization with Partially Separable Structure. *SIAM Journal on Optimization* **24**(2), 873–897 (2014), <https://epubs.siam.org/doi/abs/10.1137/130926924>
 51. Tian, Y., Chang, Y., Arias, F.H., Nieto-Granda, C., How, J.P., Carlone, L.: Kimera-Multi: Robust, Distributed, Dense Metric-Semantic SLAM for Multi-Robot Systems. *IEEE Transactions on Robotics* **38**(4), 2022–2038 (2022), <http://arxiv.org/abs/2106.14386>
 52. Tian, Y., Khosoussi, K., How, J.P.: Block-Coordinate Minimization for Large SDPs with Block-Diagonal Constraints. *arXiv:1903.00597 [cs, math]* (2019), <http://arxiv.org/abs/1903.00597>
 53. Tian, Y., Khosoussi, K., Rosen, D.M., How, J.P.: Distributed Certifiably Correct Pose-Graph Optimization. *IEEE Transactions on Robotics* **37**(6), 2137–2156 (2021), <http://arxiv.org/abs/1911.03721>
 54. Vandenberghe, L.: Chordal graphs and semidefinite optimization. *Foundations and Trends in Optimization* **1**(4), 241–433 (2015), <http://dx.doi.org/10.1561/24000000006>
 55. Wise, E., Giamou, M., Khoubyarian, S., Grover, A., Kelly, J.: Certifiably Optimal Monocular Hand-Eye Calibration. In: *IEEE International Conference on Multi-sensor Fusion and Integration for Intelligent Systems (MFI)*. pp. 271–278 (2020). <https://doi.org/10.1109/MFI49285.2020.9235219>
 56. Yang, H., Carlone, L.: Certifiably Optimal Outlier-Robust Geometric Perception: Semidefinite Relaxations and Scalable Global Optimization. *IEEE Transactions on Pattern Analysis and Machine Intelligence* **45**(3), 2816–2834 (2023), <http://arxiv.org/abs/2109.03349>
 57. Yang, H., Shi, J., Carlone, L.: TEASER : Fast and certifiable point cloud registration. *IEEE Transactions on Robotics* **32**(2), 314–333 (2020), <https://doi.org/10.1109/TR0.2020.3033695>
 58. Zheng, Y., Fantuzzi, G., Papachristodoulou, A.: Chordal and factor-width decompositions for scalable semidefinite and polynomial optimization. *Annual Reviews in Control* **52**, 243–279 (2021), <https://www.sciencedirect.com/science/article/pii/S1367578821000717>
 59. Zheng, Y., Fantuzzi, G., Papachristodoulou, A., Goulart, P., Wynn, A.: Chordal decomposition in operator-splitting methods for sparse semidefinite programs. *Mathematical Programming* **180**(1-2), 489–532 (2020), <http://link.springer.com/10.1007/s10107-019-01366-3>

A From NLS to QCQP

In this section, we give additional details concerning the reformulation of the original NLS problem to a QCQP, with a specific emphasis on retaining the sparsity of the underlying problem.

A.1 General formulation

In this section, we show how to reformulate problem (3) to a QCQP. We introduce the lifted vectors

$$\begin{aligned} \mathbf{x}_k(\boldsymbol{\xi}_k)^\top &:= [1 \ \boldsymbol{\xi}_k^\top \ \boldsymbol{\ell}_k(\boldsymbol{\xi}_k)], \\ \mathbf{x}_{ij}(\boldsymbol{\xi}_i, \boldsymbol{\xi}_j)^\top &:= [1 \ \boldsymbol{\xi}_i^\top \ \boldsymbol{\xi}_j^\top \ \boldsymbol{\ell}_i(\boldsymbol{\xi}_i) \ \boldsymbol{\ell}_j(\boldsymbol{\xi}_j)], \end{aligned} \quad (16)$$

with each $\boldsymbol{\ell}_n, n \in \mathcal{Q}$ containing N_n^s so-called substitution functions. These functions include all higher-order terms in $\boldsymbol{\xi}_i$ that appear in the cost terms, so that we can write

$$\begin{aligned} \mathbf{e}_k(\boldsymbol{\xi}_k) &= \mathbf{B}_k \mathbf{x}_k(\boldsymbol{\xi}_k), \\ \mathbf{e}_{ij}(\boldsymbol{\xi}_i, \boldsymbol{\xi}_j) &= \mathbf{B}_{ij} \mathbf{x}_{ij}(\boldsymbol{\xi}_i, \boldsymbol{\xi}_j). \end{aligned} \quad (17)$$

This allows us to rewrite the cost terms:

$$\begin{aligned} a_k(\boldsymbol{\xi}_k) &= \mathbf{x}_k(\boldsymbol{\xi}_k)^\top \underbrace{\mathbf{B}_k^\top \mathbf{W}_k \mathbf{B}_k}_{\mathbf{Q}_k} \mathbf{x}_k(\boldsymbol{\xi}_k), \\ r_{ij}(\boldsymbol{\xi}_i, \boldsymbol{\xi}_j) &= \mathbf{x}_{ij}(\boldsymbol{\xi}_i, \boldsymbol{\xi}_j)^\top \underbrace{\mathbf{B}_{ij}^\top \mathbf{W}_{ij} \mathbf{B}_{ij}}_{\mathbf{R}_{ij}} \mathbf{x}_{ij}(\boldsymbol{\xi}_i, \boldsymbol{\xi}_j), \end{aligned} \quad (18)$$

which shows that the original cost can be written as quadratic in the lifted vectors $\mathbf{x}_k(\boldsymbol{\xi}_k)$. We assume that each term of the lifted vectors can be enforced with a quadratic constraint of the form

$$\mathbf{x}_k^\top \mathbf{A}_{j_k}^s \mathbf{x}_k = b_{j_k}, \quad j_k = 1 \dots N_k^s, \quad (19)$$

which is always possible when the substitutions are polynomial or rational functions of any order.⁸ Finally, assuming that the feasible sets \mathcal{X}_n can also be characterized by a set of quadratic constraints, which we denote by \mathbf{A}_i^p , we obtain the generic equivalent QCQP formulation (5).

A.2 Example reformulations

We return to our two examples to provide specific forms of substitution functions and QCQP reformulations.

⁸ To see this, note that for an original cost of degree k , we can add all monomials up to degree k , in which case each term can be recursively constrained using its preceding terms. In practice it is often desirable to use as few higher-order terms as possible, as explained in more detail in [56].

Example CT-RO. By using just one substitution: $\ell_k(\boldsymbol{\xi}_k) := \|\mathbf{t}_k\|^2$, we get the lifted vector

$$\mathbf{x}_k(\boldsymbol{\xi}_k)^\top := [1 \ \mathbf{t}_k^\top \ \mathbf{v}_k^\top \ \|\mathbf{t}_k\|^2] \quad (20)$$

and we can write each absolute error term as

$$\begin{aligned} \mathbf{e}_k(\boldsymbol{\xi}_k)[i] &= [\tilde{d}_{ki}^2 - \|\mathbf{m}_i\|^2 \ 2\mathbf{m}_i^\top \ \mathbf{0}_3^\top \ -1] \mathbf{x}_k(\boldsymbol{\xi}_k) \\ &= \mathbf{b}_{ki}^\top \mathbf{x}_k(\boldsymbol{\xi}_{ki}) \end{aligned} \quad (21)$$

where \mathbf{b}_{ki} corresponds to one row of \mathbf{B}_k in (17). Similarly, we have:

$$\begin{aligned} \mathbf{x}_{ij}(\boldsymbol{\xi}_i, \boldsymbol{\xi}_j)^\top &= [1 \ \mathbf{t}_i^\top \ \mathbf{v}_i^\top \ \|\mathbf{t}_i\|^2 \ \mathbf{t}_j^\top \ \mathbf{v}_j^\top \ \|\mathbf{t}_j\|^2], \\ \mathbf{e}_{ij}(\boldsymbol{\xi}_i, \boldsymbol{\xi}_j) &= [\mathbf{0}_6 \ \mathbf{I}_6 \ \mathbf{0}_6 \ \boldsymbol{\Phi} \ \mathbf{0}_6] \mathbf{x}_{ij}(\boldsymbol{\xi}_i, \boldsymbol{\xi}_j). \end{aligned} \quad (22)$$

Since the substitution is the squared norm of the position, it is a polynomial and can thus be trivially written in the form (19).

Example MW. For this example, we note that the cost is already quadratic in the constraints, so no substitutions are necessary. Furthermore, the feasible set is given by $\mathcal{X}_n := SE(3)$, which can be enforced by the quadratic constraints $\mathbf{C}_{i0}^\top \mathbf{C}_{i0} = \mathbf{I}_3$ and $\mathbf{C}_{i0}[1] \times \mathbf{C}_{i0}[2] = \mathbf{C}_{i0}[3]$ (with $\mathbf{C}_{i0}[j]$ the j -th column of \mathbf{C}_{0i}), which enforces handedness and thus substitutes the (cubic) determinant constraint in the definition of $SO(3)$ [10].